$VV_2W_{10}O_{40}^{5-}$ and $VV_3W_9O_{40}^{6-}$ spectra until or unless individual isomers can be separated and identified by 2-D W NMR. We can however extrapolate from our assignments for the 1,4- and 1,4,9-isomers to estimate the chemical shifts of the currently unknown $VVW_{11}O_{40}^{4-}$: V(tetrahedral), -564 ppm; V(octahedral), -530 ppm. The 1,4,9-isomer of $PV_3W_9O_{40}^{6-}$ should have δ near -500 ppm, i.e. ~25 ppm downfield from 1,4-$PV_2W_{10}O_{40}^{5-}$,[47] and this has recently been confirmed by Domaille and Watunya.[38]

Chemical Shifts and ESR *g* Values. Some years ago Kazanskii[48] reported a linear correlation between $\delta(^{51}V)$ of four tungstovanadates, $VW_5O_{19}^{3-}$, $PVMo_{11}O_{40}^{4-}$, $PVW_{11}O_{40}^{4-}$, and $H_2VW_{11}O_{40}^{7-}$, and $\langle g \rangle$ for the corresponding anions reduced by one electron to contain vanadium(IV). Both paramagnetic nuclear shielding of V^V and the *g* value of V^{IV} are dependent upon excitation energies and orbital angular momentum, and *changes* in $\langle g \rangle$ and δ might be expected to be roughly parallel. A plot of all currently available data for polyanions that contain a single vanadium (Figure 12) shows that there is some correlation but with considerable scatter.[47]. There is no correlation for ions containing two or more vanadiums, nor is there a correlation between $\delta(^{183}W)$ for dodecatungstates and $\langle g \rangle$ for the corresponding one-electron heteropoly blues.[49]

Acknowledgment. We thank Drs. J. Wooten, W. Egan, R. Johanneson, and L. Baltzer for the use of spectrometers and for helpful advice and Professor C. F. Hammer for many discussions and suggestions. The research has been supported by the NSF through Grant Nos. CHE8019039 and CHE8306736.

(48) Kazanskii, L. P.; Spitsyn, V. I. *Dokl. Phys. Chem. (Engl. Transl.)* **1975**, *223*, 721.

(49) (a) Acerete, R.; Hammer, C. F.; Baker, L. C. W. *J. Am. Chem. Soc.* **1982**, *104*, 5384. (b) Prados, R. A.; Pope, M. T. *Inorg. Chem.* **1976**, *15*, 2547.

Contribution from the Department of Chemistry, University of Rochester, Rochester, New York 14627

Preparation and Structural Examination of a Series of New, Low-Valent Iron Phosphine Isocyanide Complexes with Bent C-N-C Linkages

William D. Jones,*† Glenn P. Foster, and Jeanne M. Putinas

Received October 27, 1986

A general synthesis for the preparation of complexes with the formula $Fe(PMe_3)_2(CNR)_3$ where R = Me, Et, *i*-Pr, *t*-Bu, CH_2CMe_3, Ph, and 2,6-xylyl (2,6-xyl) is reported from the reaction of $Fe(PMe_3)_4$ with isocyanides. The derivatives with R = CH_2CMe_3, Ph, and 2,6-xyl have been structurally characterized. $Fe(PMe_3)_2(CNCH_2CMe_3)_3$ crystallizes in monoclinic space group *C*2 with $Z = 4$ and with $a = 28.645$ (13) Å, $b = 9.590$ (4) Å, $c = 11.983$ (4) Å, $\beta = 101.36$ (3)°, and $V = 3227.0$ (4.2) Å^3. $Fe(PMe_3)_2(CNPh)_3$ crystallizes in monoclinic space group $C2/c$ with $Z = 4$ and with $a = 14.136$ (9) Å, $b = 11.559$ (12) Å, $c = 17.343$ (9) Å, $\beta = 98.19$ (4)°, and $V = 2804.9$ (6.4) Å^3. $Fe(PMe_3)_2(CN\text{-}2,6\text{-}xyl)_3$ crystallizes in monoclinic space group $P2_1/c$ with $Z = 4$ and with $a = 9.542$ (2) Å, $b = 24.086$ (5) Å, $c = 15.473$ (5) Å, $\beta = 105.61$ (2)°, and $V = 3424.9$ (2.9) Å^3. These complexes undergo equilibrium exchange reactions with added RNC in solution, giving products with the stoichiometry $Fe(PMe_3)(CNR)_4$ and $Fe(CNR)_5$. The complex $Fe(PMe_3)(CN\text{-}2,6\text{-}xyl)_4$ has been structurally characterized and crystallizes in space group $P2_1/c$ with $Z = 4$ and with $a = 21.655$ (4) Å, $b = 9.901$ (3) Å, $c = 19.609$ (3) Å, $\beta = 113.30$ (1)°, and $V = 3861.6$ (3.3) Å^3. These structures are compared and contrasted with other known structures of $Ru(PPh_3)(CNR)_4$ and $Fe(CNR)_5$ complexes. A general feature observed is the markedly increased bending of the C-N-C linkage upon decreasing the number of π-acceptor RNC ligands.

Introduction

Many inorganic and organometallic complexes of metals in low oxidation states are known in which the ligand set is comprized of good π-acceptor ligands. Delocalization of electron density into the ligands tends to render the metal less reducing (lowering its reduction potential) and consequently less reactive toward air, water, and other small unsaturated molecules. While carbon monoxide is a π-acceptor that is commonly used for this purpose, the isoelectronic isocyanide ligand also "stabilizes" metals in low oxidation states by lowering their reduction potentials.

In 1975, simultaneous reports appeared from Muetterties and Klein regarding the reduction of $FeCl_2$ in the presence of PMe_3.[1,2] An unstable complex could be isolated and characterized with the empirical formula $[Fe(PMe_3)_4]$. Further studies of this complex revealed a dynamic process in which this 16-electron Fe(0) species was in fact in equilibrium with the intramolecular oxidative-addition adduct $HFe(PMe_2CH_2)(PMe_3)_3$. Evidence for the presence of a facile equilibrium was also provided by a series of reactions of the incipient coordinatively unsaturated complex with σ-donor ligands and oxidative-addition substrates (Scheme I).[3]

Scheme I

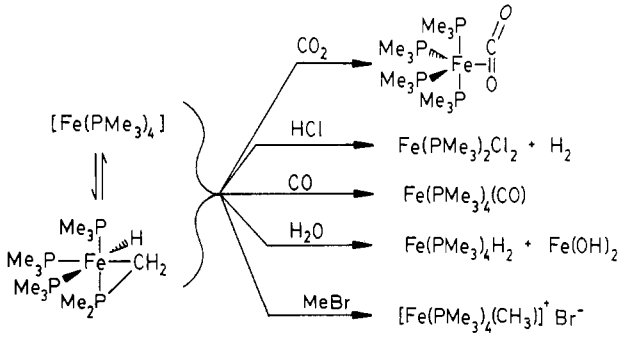

In this paper, we report the preparation and structures of a series of new, low-valent iron(0) complexes containing both PMe_3 and RNC ligands that are active in C-H bond functionalization reactions.[4] Earlier studies of the reduction of iron(II) isocyanide

† A. P. Sloan Fellow, 1984-1986. Camille and Henry Dreyfus Teacher Scholar, 1985-1987.

(1) Rathke, J. W.; Muetterties, E. L. *J. Am. Chem. Soc.* **1975**, *97*, 3272-3273.

(2) Karsch, H. H.; Klein, H. F.; Schmidbaur, H. *Chem. Ber.* **1977**, *110*, 2200-2212. Karsch, H. H. *Inorg. Synth.* **1977**, *20*, 69-75. Karsch, H. H.; Klein, H.-F.; Schmidbaur, H. *Angew. Chem., Int. Ed. Engl.* **1975**, *14*, 637-638.

(3) Karsch, H. H. *Chem. Ber.* **1977**, *110*, 2213-2221. Karsch, H. H. *Chem. Ber.* **1977**, *110*, 2699-2711. Karsch, H. H. *Chem. Ber.* **1977**, *110*, 2712-2720.

0020-1669/87/1326-2120$01.50/0

or phosphine complexes allowed the synthesis and structural characterization of $Fe(CN\text{-}t\text{-}Bu)_5$,[5] $Ru(CN\text{-}t\text{-}Bu)_5$,[6] and $Ru(PPh_3)(CN\text{-}t\text{-}Bu)_4$.[7] The present study extends the range of these complexes to provide examples with the better σ-donating phosphine PMe_3 of the formula $Fe(PMe_3)_2(CNR)_3$. Evidence for the production of $Fe(PMe_3)_3(CNR)_2$ is also provided.

Results

Preparation of a dark brown THF solution of the complex $[Fe(PMe_3)_4]$ followed by treatment with 3.5 equiv of isocyanide results in the formation of an orange solution containing the new complex $Fe(PMe_3)_2(CNR)_3$ (eq 1). These complexes are easily

$$[Fe(PMe_3)_4] + CNR \rightarrow Fe(PMe_3)_2(CNR)_3 + PMe_3 \quad (1)$$

isolated in crude form in ~50% yield by evaporation of solvent under vacuum and extraction of the residue with hexane or toluene. Recrystallization at low temperature is the optimal method for obtaining pure product as the complexes decompose upon chromatography on silica. Using fewer equivalents of isocyanide results in poor product yields due to contamination of the $Fe(PMe_3)_2(CNR)_3$ product with unreacted (and thermally unstable) $[Fe(PMe_3)_4]$, and using a greater number of equivalents gives contamination with more highly isocyanide substituted products (vide infra).

All of the complexes are extremely air sensitive but are only moderately thermally stable at room temperature, with stability decreasing according to the sequence R = 2,6-xylyl (2,6-xyl) = Ph > CH_2CMe_3 > *t*-Bu > Me ≫ *i*-Pr > Et. For the reactions with ethyl or isopropyl isocyanide, a crystalline product could not be obtained despite the presence of the bright orange solution characteristic of the formation of $Fe(PMe_3)_2(CNR)_3$. The complex with R = Me decomposes slowly over several days at 25 °C, and with R = *t*-Bu the complex is stable for weeks. The complexes with R = *i*-Pr or Et could not be isolated, although their formation and decomposition were evident. With R = *i*-Pr, solvent evaporation cools the solution and leaves behind an orange solid that decomposes with gas evolution upon warming to room temperature. Trapping these gases in C_6H_6 at 77 K followed by GC analysis shows the presence of propene and PMe_3, but no *i*-PrNC. With ethyl isocyanide, a black residue forms upon evaporation of solvent.

Attempts to prepare the complex in a single step by coreduction of a THF solution of PMe_3, RNC, and $FeCl_2$ in the presence of Mg fail due to the formation of nonreactive $FeCl_2(PMe_3)_2(CNR)_2$ species, analogous to the previous studies by Malatesta.[8] Stronger reducing agents such as Na/Hg do not yield product.

All of the complexes display similar ^1H NMR spectra with resonances for three equivalent isocyanide ligands and a pseudotriplet for the two equivalent PMe_3 ligands. The isocyanide ligands with α-CN hydrogens (CNMe, $CNCH_2CMe_2$) show a coupling between these hydrogen atoms and the phosphorus nuclei, the multiplicity of which correlates with the number of PMe_3 ligands. Data are summarized in Table I. They crystallize readily from hydrocarbon solution at low temperature, giving large needle-shaped crystals that, after cleaving, are suitable for single-crystal X-ray structural studies. The complexes with R = CH_2CMe_3, Ph, and 2,6-xyl have been examined as outlined below.

Following standard data collection on the complex $Fe(PMe_3)_2(CNCH_2CMe_3)_3$ in accordance with the parameters in Table II, a Patterson map revealed the iron atom in a general position. Subsequent difference Fourier maps and isotropic least-squares refinements revealed all atoms in the molecule,

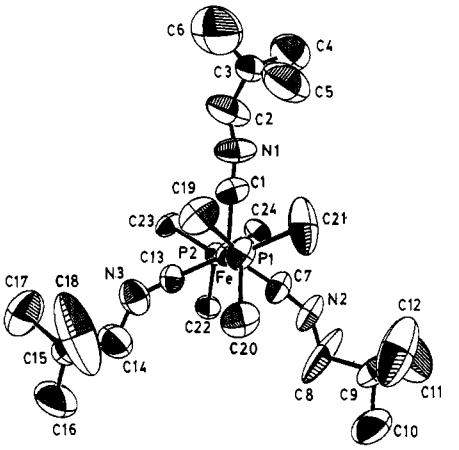

Figure 1. ORTEP drawing of $Fe(PMe_3)_2(CNCH_2CMe_3)_3$. Ellipsoids are shown at the 30% probability level.

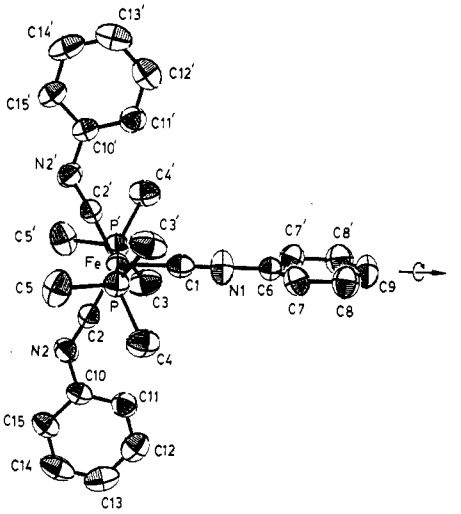

Figure 2. ORTEP drawing of $Fe(PMe_3)_2(CNPh)_3$. Ellipsoids are shown at the 50% probability level.

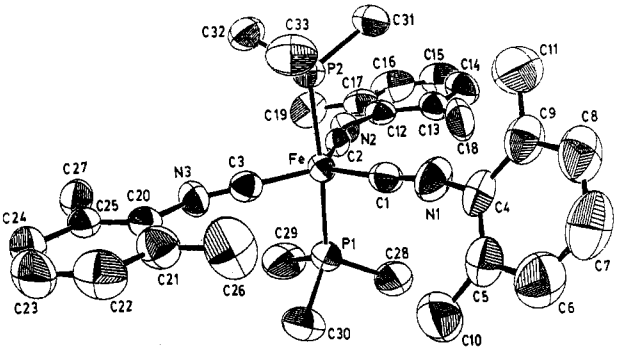

Figure 3. ORTEP drawing of $Fe(PMe_3)_2(CN\text{-}2,6\text{-}xyl)_3$. Ellipsoids are shown at the 50% probability level.

although the thermal parameters for the neopentyl methyl groups were rather large (B = 10–20 Å^2). Anisotropic refinement converged with R_1 = 0.065 and R_2 = 0.079. A final difference Fourier map showed small regions of electron density near the neopentyl methyl groups, but no obvious disorder could be ascertained to account for the large thermal parameters for these atoms. The structural data are therefore best interpreted in terms of large thermal motions of the nearly spherical CH_2CMe_3 group rather than rotational disorder about the CH_2–CMe_3 axis. Figure 1 shows an ORTEP drawing of the molecule, Table III gives selected distances and angles, and Table IV lists fractional atomic coordinates.

$Fe(PMe_3)_2(CNPh)_3$ was also examined structurally. Data collection as outlined in Table II followed by Patterson map

(4) Jones, W. D.; Foster, G. P.; Putinas, J. M. *J. Am. Chem. Soc.*, in press.
(5) Bassett, J.-M.; Green, M.; Howard, J. A. K.; Stone, F. G. A. *J. Chem. Soc., Chem. Commun.* **1977**, 853–854.
(6) Barker, G. K.; Galas, A. M. R.; Green, M.; Howard, J. A. K.; Stone, F. G. A.; Turney, T. W.; Welch, A. J.; Woodward, P. *J. Chem. Soc., Chem. Commun.* **1977**, 256–257.
(7) Bassett, J.-M.; Berry, D. E.; Barker, G. K.; Green, M.; Howard, J. A. K.; Stone, F. G. A. *J. Chem. Soc., Dalton Trans.* **1979**, 1003–1011.
(8) Malatesta, L.; Bonati, F. *Isocyanide Complexes of Transition Metals*; Wiley: New York, 1969. See also: Karsch, H. H. *Chem. Ber.* **1977**, *110*, 2222–2235.

Table I. ^{1}H NMR Data for Iron Isocyanide Compounds in C_6D_6[a]

compd	PMe_3 resonance	CNR resonance(s)
$Fe(PMe_3)_2(CNMe)_3$	1.477 (pt, J = 3.6 Hz, 18 H)	2.820 (t, J = 2.5 Hz, 9 H)
$Fe(PMe_3)_2(CN\text{-}t\text{-}Bu)_3$	1.547 (pt, J = 3.7 Hz, 18 H)	1.264 (s, 27 H)
$Fe(PMe_3)_2(CNCH_2CMe_3)_3$	1.589 (pt, J = 3.7 Hz, 18 H)	3.134 (t, J = 2.7 Hz, 6 H) 0.905 (s, 27 H)
$Fe(PMe_3)_2(CNPh)_3$	1.457 (pt, J = 3.9 Hz, 18 H)	7.301 (d, J = 7.4 Hz, 6 H) 7.052 (t, J = 7.8 Hz, 6 H) 6.870 (t, J = 7.4 Hz, 3 H)
$Fe(PMe_3)_2(CN\text{-}2,6\text{-}xyl)_3$	1.455 (pt, J = 2.7 Hz, 18 H)	2.496 (s, 18 H) 6.92 (m, 6 H) 6.84 (m, 3 H)
$Fe(PMe_3)(CN\text{-}t\text{-}Bu)_4$	1.470 (d, J = 8.5 Hz, 9 H)	1.297 (s, 36 H)
$Fe(PMe_3)(CNCH_2CMe_3)_4$	1.561 (d, J = 8.8 Hz, 9 H)	3.089 (d, J = 1.0 Hz, 8 H) 0.956 (s, 36 H)
$Fe(PMe_3)(CN\text{-}2,6\text{-}xyl)_4$	1.549 (d, J = 9 Hz, 9 H)	2.445 (s, 24 H) 6.813 (m, 12 H)
$Fe(PMe)_3(CNCH_2CMe_3)_2$	1.374 (pt, J = 3.0 Hz, 27 H)	3.270 (q, J = 2.4 Hz, 4 H) 0.981 (s, 18 H)
$Fe(CN\text{-}t\text{-}Bu)_5$		1.278 (s)
$Fe(CNCH_2CMe_3)_5$		3.056 (s, 10 H) 0.966 (s, 45 H)

[a] pt = pseudotriplet, t = triplet, d = doublet, s = singlet, m = multiplet

solution showed the iron atom on a 2-fold axis. Routine difference Fourier methods revealed the entire molecule with one of the three equatorial isocyanide ligands lying along the 2-fold axis, and therefore constrained to be perfectly linear. This geometry is shown in Figure 2, and distances and angles as well as fractional atomic coordinates are listed in Tables III and V.

The related complex $Fe(PMe_3)_2(CN\text{-}2,6\text{-}xyl)_3$ was also examined structurally. Data collection as outlined in Table II followed by Patterson map solution showed the iron atom in a general position. Routine difference Fourier methods revealed the entire molecule with a trigonal-bipyramidal geometry, as shown in Figure 3. Distances and angles are given in Table III, and fractional atomic coordinates are listed in Table VI.

These complexes were found to partake in thermal substitution equilibria in benzene solution at 25 °C. Treatment of a solution of $Fe(PMe_3)_2(CN\text{-}t\text{-}Bu)_3$ with t-BuNC in C_6D_6 solution results in the formation of an equilibrium mixture including $Fe(PMe_3)(CN\text{-}t\text{-}Bu)_4$ and $Fe(CN\text{-}t\text{-}Bu)_5$ after a few hours. ^{1}H NMR integration of the t-BuNC and PMe_3 resonances, both free and bound, allows facile measurement of the equilibrium constants defined in eq 2 and 3. For R = t-BuNC, K_1 = 0.035 (5) and

$$Fe(PMe_3)_2(CNR)_3 + \overset{K_1}{\rightleftharpoons} Fe(PMe_3)(CNR)_4 + PMe_3 \quad (2)$$

$$Fe(PMe_3)(CNR)_4 + RNC \overset{K_2}{\rightleftharpoons} Fe(CNR)_5 + PMe_3 \quad (3)$$

K_2 = 0.0079 (24). Similar equilibria were observed with other isocyanide ligands. For R = CH_2CMe_3, K_1 = 0.124 (9) and K_2 = 0.0447 (4).

As with the $Fe(PMe_3)_2(CNR)_3$ derivatives, the complexes $Fe(PMe_3)(CNR)_4$ show simple ^{1}H NMR spectra with equivalent isocyanide ligands. The complex with R = 2,6-xyl was found to crystallize nicely and was examined structurally. Routine data collection according to the parameters in Table II followed by Patterson map solution in space group $P2_1/c$ revealed the iron atom in a general position. Difference Fourier maps were used to locate the remaining atoms. Anisotropic refinement was carried

Table II. Summary of Crystallographic Data[a]

	crystal parameters			
	I	II	III	IV
formula	$FeP_2N_3C_{24}H_{51}$	$FeP_2N_3C_{27}H_{33}$	$FeP_2N_3C_{33}H_{45}$	$FePN_4C_{42}H_{48}$
fw	499.49	517.38	601.54	695.70
cryst system	monoclinic	monoclinic	monoclinic	monoclinic
space group	$C2$ (No. 5)	$C2/c$ (No. 15)	$P2_1/c$ (No. 14)	$P2_1/c$
Z	4	4	4	4
a, Å	28.645 (13)	14.136 (9)	9.542 (2)	21.655 (4)
b, Å	9.590 (4)	11.559 (12)	24.086 (5)	9.901 (3)
c, Å	11.983 (4)	17.343 (9)	15.473 (5)	19.609 (3)
β, deg	101.36 (3)	98.19 (4)	105.61 (2)	113.30 (1)
vol, Å^3	3227.0 (4.2)	2804.9 (6.4)	3424.9 (2.9)	3861.6 (3.3)
d_{calcd}, g/cm^3	1.028	1.225	1.167	1.197
cryst dimens, mm	0.30 × 0.52 × 0.60	0.10 × 0.20 × 0.25	0.34 × 0.45 × 0.60	0.15 × 0.30 × 0.56
temp, °C	25	25	25	25
diffractometer	CAD4	FACS1	CAD4	CAD4
radiation (mono)	Mo (graphite)	Mo (graphite)	Mo (graphite)	Mo (graphite)
scan type	$2\theta/\omega$	$2\theta/\omega$	$2\theta/\omega$	$2\theta/\omega$
scan rate, deg/min	2.0–16.5	2.0	2.0–16.5	2.0–16.5
total bkgd time	scan time/2	30 s	scan time/2	scan time/2
takeoff angle, deg	2.6	2.6	2.6	2.6
scan range, deg	0.7 + 0.35 tan θ	0.7	0.6 + 0.35 tan θ	0.65 + 0.35 tan θ
2θ range, deg	4–48	2–45	4–44	4–48
data collected	$+h,+k,\pm l$	$\pm h,+k,+l$	$+h,+k,\pm l$	$+h,+k,\pm l$
no. of data collected	2757	2064	4620	6630
no. of unique data > 3σ	1804	1271	3097	2514
no. of params varied	270	152	352	433
abs coeff, cm^{-1}	8.62	6.66	5.54	4.62
systematic absences	hkl, $h + k$ odd	hkl, $h + k$ odd; $0kl$, l odd	$0k0$, k odd; $h0l$, l odd	$0k0$, k odd; $h0l$, l odd
abs cor	empirical	none	none	none
range of transmission factors	94.0–100.0			
equiv data	$0kl = 0k\bar{l}$	$hk0 = \bar{h}k0$	$0kl = 0k\bar{l}$	$0kl = 0k\bar{l}$
agreement between equiv data (F_o)	0.036	0.030	0.024	0.025
R_1[b]	0.065	0.035	0.038	0.046
R_2[b]	0.079	0.045	0.052	0.049
goodness of fit	2.77	1.58	1.87	1.32

[a] Key: $Fe(PMe_3)_2(CNCH_2CMe_3)_3$, I; $Fe(PMe_3)_2(CNPh)_3$, II; $Fe(PMe_3)_2(CN\text{-}2,6\text{-}xyl)_3$, III; $Fe(PMe_3)(CN\text{-}2,6\text{-}xyl)_4 \cdot {}^1/_2C_6H_6$, IV. [b] R_1 and R_2 are as defined in ref 13.

Table III. Selected Distances (Å) and Angles (deg)

bond	distance	bond	angle	bond	angle
		$Fe(PMe_3)_2(CNCH_2CMe_3)_3$			
Fe–P1	2.196 (2)	P1–Fe–P2	179.45 (9)	C1–Fe–C7	118.7 (5)
Fe–P2	2.155 (2)	P1–Fe–C1	90.1 (2)	C1–Fe–C13	117.9 (4)
Fe–C1	1.826 (10)	P1–Fe–C7	89.8 (3)	C7–Fe–C13	123.4 (4)
Fe–C7	1.764 (9)	P1–Fe–C13	88.8 (3)	C1–N1–C2	166. (1)
Fe–C13	1.747 (9)	P2–Fe–C1	90.0 (2)	C7–N2–C8	146. (2)
		P2–Fe–C7	90.6 (3)	C13–N3–C14	140. (1)
		P2–Fe–C13	90.7 (3)		
		$Fe(PMe_3)_2(CNPh)_3$			
Fe–P	2.186 (2)	P–Fe–P′	178.84 (7)	C1–Fe–C2	116.9 (1)
Fe–C1	1.814 (6)	P–Fe–C1	90.58 (4)	C2–Fe–C2′	126.2 (2)
Fe–C2	1.769 (4)	P–Fe–C2	89.3 (1)	C1–N1–C6	180. (0)
		P′–Fe–C2	90.1 (1)	C2–N2–C10	131.8 (3)
		$Fe(PMe_3)_2(CN\text{-}2,6\text{-}xyl)_3$			
Fe–P1	2.189 (2)	P1–Fe–P2	173.73 (3)	C1–Fe–C2	117.1 (1)
Fe–P2	2.189 (1)	P1–Fe–C1	96.29 (9)	C1–Fe–C3	177.6 (1)
Fe–C1	1.801 (3)	P1–Fe–C2	86.81 (9)	C2–Fe–C3	125.2 (1)
Fe–C2	1.770 (3)	P1–Fe–C3	88.67 (9)	C1–N1–C4	161.3 (3)
Fe–C3	1.793 (3)	P2–Fe–C1	89.97 (9)	C2–N2–C12	147.7 (3)
		P2–Fe–C2	90.05 (9)	C3–N3–C20	149.8 (3)
		P2–Fe–C3	88.71 (9)		
		$Fe(PMe_3)(CN\text{-}2,6\text{-}xyl)_4$			
Fe–P1	2.190 (2)	P1–Fe–C1	176.1 (2)	C2–Fe–C3	117.5 (2)
Fe–C1	1.819 (7)	P1–Fe–C2	88.3 (2)	C2–Fe–C4	126.1 (2)
Fe–C2	1.831 (6)	P1–Fe–C3	90.7 (2)	C3–Fe–C4	116.1 (2)
Fe–C3	1.823 (6)	P1–Fe–C4	86.6 (2)	C1–N1–C5	174.5 (6)
Fe–C4	1.802 (6)	C1–Fe–C2	89.3 (2)	C2–N2–C13	167.9 (6)
		C1–Fe–C3	93.2 (3)	C3–N3–C21	166.7 (6)
		C1–Fe–C4	92.3 (3)	C4–N4–C29	145.1 (6)

Table IV. Positional Parameters for $Fe(PMe_3)_2(CNCH_2CMe_3)_3$

atom	x	y	z
Fe	0.15730 (4)	0.000	0.1229 (1)
P1	0.1200 (1)	0.1820 (3)	0.1739 (3)
P2	0.19400 (8)	−0.1776 (3)	0.0714 (2)
N1	0.7481 (4)	0.585 (1)	0.280 (1)
N2	0.5899 (3)	0.306 (1)	0.2013 (9)
N3	0.3625 (4)	0.606 (1)	0.1108 (8)
C1	0.2120 (4)	0.055 (1)	0.219 (1)
C2	0.7871 (6)	0.622 (2)	0.320 (1)
C3	0.8010 (5)	0.709 (2)	0.423 (1)
C4	0.1781 (5)	0.603 (3)	0.479 (1)
C5	0.2537 (9)	0.270 (4)	0.475 (2)
C6	0.349 (1)	0.256 (4)	0.406 (3)
C7	0.6177 (4)	0.389 (1)	0.1760 (9)
C8	0.5511 (5)	0.230 (3)	0.165 (2)
C9	0.5157 (5)	0.217 (2)	0.255 (1)
C10	0.9680 (7)	0.673 (3)	0.173 (2)
C11	0.031 (1)	0.603 (2)	0.337 (2)
C12	0.5111 (8)	0.344 (2)	0.335 (2)
C13	0.1464 (3)	0.064 (1)	−0.0163 (8)
C14	0.3957 (6)	0.591 (2)	0.206 (1)
C15	0.4039 (4)	0.714 (1)	0.290 (1)
C16	0.437 (1)	0.654 (4)	0.383 (2)
C17	0.3501 (6)	0.732 (3)	0.342 (2)
C18	0.913 (1)	0.337 (2)	0.215 (2)
C19	0.1442 (5)	0.353 (1)	0.157 (1)
C20	0.0557 (4)	0.199 (2)	0.100 (1)
C21	0.6186 (6)	0.690 (2)	0.328 (1)
C22	0.1586 (4)	−0.295 (1)	−0.0325 (8)
C23	0.2448 (3)	−0.143 (1)	0.006 (1)
C24	0.2188 (4)	−0.303 (1)	0.1820 (9)

out to $R_1 = 0.046$ and $R_2 = 0.049$. Listings of distances and angles are given in Table III, and fractional atomic coordinates in Table VII.

Irradiation of a benzene solution of $Fe(PMe_3)_2(CNCH_2CMe_3)_3$ in the presence of added PMe_3 results in the formation of free $CNCH_2CMe_3$ and a new species in ~30% yield possessing a quartet at δ 3.270 (J = 2.4 Hz, 4 H), a pseudotriplet at δ 1.374 (J = 3.0 Hz, 27 H), and a singlet at δ 0.981 (18 H). The ^{31}P NMR spectrum showed a singlet at δ 29.28. The complex is very air sensitive and could not be isolated in pure form. On the basis

Table V. Positional Parameters for $Fe(PMe_3)_2(CNPh)_3$

atom	x	y	z
Fe	0.0 (0)	0.07409 (7)	0.250 (0)
P1	0.09689 (7)	0.07214 (10)	0.16236 (6)
C1	0.0 (0)	0.2311 (6)	0.250 (0)
N1	0.0 (0)	0.3332 (5)	0.250 (0)
C2	0.08896 (27)	0.0049 (3)	0.31614 (22)
N2	0.14808 (24)	−0.04997 (28)	0.36015 (21)
C3	0.0508 (3)	0.1397 (4)	0.06984 (24)
C4	0.2094 (3)	0.1461 (5)	0.18815 (27)
C5	0.1337 (3)	−0.0690 (4)	0.1332 (3)
C6	0.0 (0)	0.4518 (5)	0.250 (0)
C7	0.05177 (29)	0.5115 (4)	0.20098 (28)
C8	0.0504 (3)	0.6308 (4)	0.2017 (3)
C9	0.0 (0)	0.6907 (5)	0.250 (0)
C10	0.22571 (27)	−0.0143 (4)	0.41475 (22)
C11	0.27935 (29)	−0.0977 (4)	0.45846 (24)
C12	0.3560 (3)	−0.0653 (5)	0.51371 (28)
C13	0.3799 (3)	0.0490 (5)	0.52415 (29)
C14	0.3269 (4)	0.1319 (4)	0.4795 (3)
C15	0.2505 (3)	0.1016 (4)	0.42529 (25)

of the ^1H NMR spectrum and the coupling patterns, the complex is assigned the formula $Fe(PMe_3)_3(CNCH_2CMe_3)_2$ (eq 4).

$$Fe(PMe_3)_2(CNCH_2CMe_3)_3 \xrightarrow[PMe_3]{h\nu} Fe(PMe_3)_3(CNCH_2CMe_3)_2 \quad (4)$$

Discussion

The formation of five-coordinate trigonal-bipyramidal molecules from $[Fe(PMe_3)_4]$ is not surprising in light of the coordinative unsaturation of the starting complex. While the intermediates $Fe(PMe_3)_4(CNR)$ and $Fe(PMe_3)_3(CNR)_2$ were not observed when less than 3 equiv of isocyanide was used in the preparation, their intermediacy is highly likely in view of the observed equilibria between the more substituted species.

The equilibrium constants measured indicate a thermodynamic preference for the formation of the bis(phosphine) tris(isocyanide) complex when equal amounts of PMe_3 and isocyanide are present. This ligand combination apparently balances the electron richness of the iron(0) metal center and its good electron-donor PMe_3 ligands with the π-acceptor ability of the isocyanide ligand.

Table VI. Positional Parameters for $Fe(PMe_3)_2(CN\text{-}2,6\text{-}xyl)_3$

atom	x	y	z
Fe	−0.00919 (5)	0.14050 (2)	0.06381 (3)
P1	−0.1314 (1)	0.15465 (4)	0.16289 (7)
P2	0.1078 (1)	0.11668 (4)	−0.03436 (6)
N1	0.0877 (4)	0.2573 (1)	0.0497 (2)
N2	0.1859 (3)	0.0690 (1)	0.2027 (2)
N3	−0.2849 (3)	0.0995 (1)	−0.0632 (2)
C1	0.0434 (4)	0.2115 (2)	0.0652 (2)
C2	0.1109 (4)	0.0988 (1)	0.1464 (2)
C3	−0.1749 (4)	0.1172 (1)	−0.0133 (2)
C4	0.0954 (4)	0.3125 (2)	0.0261 (2)
C5	−0.0154 (5)	0.3482 (2)	0.0311 (3)
C6	−0.0033 (6)	0.4037 (2)	0.0081 (4)
C7	0.1134 (6)	0.4216 (2)	−0.0186 (4)
C8	0.2212 (5)	0.3860 (2)	−0.0227 (3)
C9	0.2160 (5)	0.3310 (2)	−0.0004 (3)
C10	−0.1438 (5)	0.3287 (2)	0.0635 (4)
C11	0.3360 (5)	0.2921 (2)	−0.0043 (3)
C12	0.3136 (4)	0.0635 (2)	0.2720 (2)
C13	0.4118 (4)	0.1076 (2)	0.2956 (2)
C14	0.5397 (5)	0.0985 (3)	0.3611 (3)
C15	0.5684 (5)	0.0485 (3)	0.4024 (3)
C16	0.4704 (5)	0.0056 (2)	0.3805 (3)
C17	0.3411 (4)	0.0122 (2)	0.3144 (2)
C18	0.3793 (5)	0.1635 (2)	0.2517 (3)
C19	0.2348 (5)	−0.0337 (2)	0.2893 (3)
C20	−0.4100 (4)	0.1079 (2)	−0.1329 (2)
C21	−0.4434 (4)	0.1603 (2)	−0.1714 (3)
C22	−0.5709 (5)	0.1650 (2)	−0.2411 (3)
C23	−0.6594 (5)	0.1210 (2)	−0.2701 (3)
C24	−0.6252 (4)	0.0697 (2)	−0.2314 (3)
C25	−0.5002 (3)	0.0624 (2)	−0.1617 (2)
C26	−0.3484 (6)	0.2090 (2)	−0.1411 (4)
C27	−0.4618 (4)	0.0070 (2)	−0.1191 (3)
C28	−0.0430 (5)	0.1936 (2)	0.2617 (3)
C29	−0.1826 (5)	0.0918 (2)	0.2103 (3)
C30	−0.3046 (5)	0.1905 (2)	0.1270 (3)
C31	0.3031 (4)	0.1290 (2)	−0.0027 (3)
C32	0.0986 (4)	0.0440 (2)	−0.0667 (3)
C33	0.0492 (5)	0.1511 (2)	−0.1426 (3)

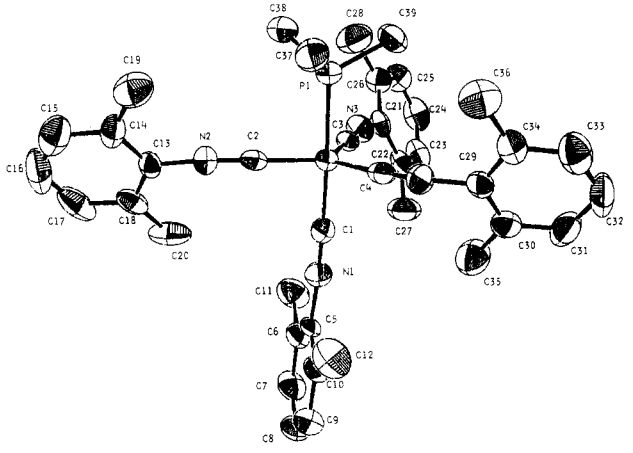

Figure 4. ORTEP drawing of $Fe(PMe_3)(CN\text{-}2,6\text{-}xyl)_4$. Ellipsoids are shown at the 50% probability level.

The structural examinations of the molecules all display the nearly perfect trigonal-bipyramidal geometries anticipated for d^8 five-coordinate molecules. In comparing these structures with the earlier reports on $Fe(t\text{-}BuNC)_5$ and $Fe(PPh_3)(t\text{-}BuNC)_4$, one observes trigonal-bipyramidal structures throughout with equatorial *t*-BuNC ligands. While there is no structural information for the hypothetical molecule $Fe(PMe_3)_5$, and the known complexes $Fe(PMe_3)_3(PMe_2CH_2PMe_2)$ and $Fe(dmpe)_2(PEt_3)$ have not been structurally characterized,[9] the related $Ru(PMe_2CH_2CH_2PMe_2)_2(PMe_3)$ complex unexpectedly displayed a square-pyramidal geometry.[10] Exchange of the PMe_3 ligand for CO in this ruthenium molecule changes the structure to a trigonal bipyramid.[10]

The unique structural feature of the molecules reported here appears in the form of a severe bending of the C–N–C linkage. Table VIII lists these angles for a variety of isocyanide molecules.[11] As can be seen, the complexes in this report are among the smallest C–N–C angles in the list. There is a general tendency for two of the isocyanide ligands to display a higher degree of bending than the third in the $Fe(PMe_3)_2(CNR)_3$ molecules. This feature is exemplified by comparing the structures of $Fe(PMe_3)_2(CNPh)_3$ and $Fe(PMe_3)_2(CN\text{-}2,6\text{-}xyl)_3$. The former contains one RNC ligand that is crystallographically constrained to be linear, leaving the remaining two to take up the excess metal electron density and therefore display a high degree of C–N–C bending. The latter complex lies in a general position and the accommodation of electron density (and C–N–C bending) is distributed over all three RNC ligands. The PMe_3 ligands always occupy the axial positions.

Comparison of the previously characterized complex $Ru(PPh_3)(CN\text{-}t\text{-}Bu)_4$[7] with $Fe(PMe_3)(CN\text{-}2,6\text{-}xyl)_4$ shows a similar degree of C–N–C bending despite the presence of a less electron donating PPh_3 ligand, although the ruthenium complex displays a distorted trigonal-bipyramidal geometry in which the phosphine occupies an equatorial position. $Fe(CN\text{-}t\text{-}Bu)_5$ also displays strong bending of the C–N–C linkage in a distorted trigonal-bipyramidal geometry.[7] $Fe(CN\text{-}2,6\text{-}xyl)_5$, also prepared[7] but not structurally characterized, was postulated to possess linear M–CNR ligands on the basis of its IR spectrum. The related d^8 derivative $[Co(CNMe)_5]^+$ also shows a trigonal-bipyramidal structure with minimal (<3°) deviation of the C–N–C angles from linearity.[11m] The structures reported here suggest that this complex probably also has strongly bent C–N–C linkages.

Another interesting feature of the structures of the $Fe(PMe_3)_2(CNR)_3$ molecules is that the direction of the CNR bending is always in the equatorial plane. This observation can be accounted for in terms of decreased steric interference in this plane, although examination of the resonance structure for M–CNR π-back-bonding as shown below indicates that in-plane bending will result in maximum interaction of the CNR π^* orbital with the highest energy filled d_{xy} and $d_{x^2-y^2}$ metal orbitals.

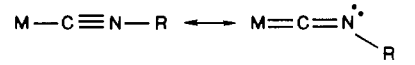

Examination of the IR spectra of these Fe(0) derivatives also shows an interesting feature. They all possess broad, low-energy (<2000 cm^{-1}) C≡N stretches as opposed to the typical RNC stretches in other complexes (~2100 cm^{-1}). This common feature can be explained in terms of the limiting pseudoresonance form for the π-acceptor ligand indicated above. Formation of a metal–isocyanide ligand π-bond induces bending of the C–N–C linkage as the nitrogen changes from sp to sp^2 hybridization. The

(9) (a) Karsch, H. H. *Angew. Chem., Int. Ed. Engl.* **1982**, *21*, 311–312. (b) Ittel, S. D.; Tolman, C. A.; English, A. D.; Jesson, J. P. *J. Am. Chem. Soc.* **1976**, *98*, 6073–6075.

(10) Jones, W. D.; Libertini, E. *Inorg. Chem.* **1986**, *25*, 1794–1800.

(11) (a) Chatt, J.; Pombeiro, A. J. L.; Richards, R. L.; Royston, G. H. D.; Muir, K. W.; Walker, R. *J. Chem. Soc., Chem. Commun.* **1975**, 708–709. (b) Francis, C. G.; Khan, S. I.; Morton, P. R. *Inorg. Chem.* **1984**, *23*, 3680–3681. (c) Green, M.; Howard, J. A. K.; Spencer, J. L.; Stone, F. G. A. *J. Chem. Soc., Chem. Commun.* **1975**, 3–4. Green, M.; Howard, J. A. K.; Murray, M.; Spencer, J. L.; Stone, F. G. A. *J. Chem. Soc., Dalton Trans.* **1977**, 1509–1514. (d) Day, V. W.; Day, R. O.; Kristoff, J. S.; Hirsekorn, F. J.; Muetterties, E. L. *J. Am. Chem. Soc.* **1975**, *97*, 2571–2573. (e) Yamamoto, Y.; Aoki, K.; Yamazaki, H. *Organometallics* **1983**, *2*, 1377–1381. (f) Gambarotta, S.; Floriani, C.; Chiesi-Villa, A.; Guastini, C. *Inorg. Chem.* **1984**, *23*, 1739–1747. (g) Dewan, J. C.; Mialki, W. S.; Walton, R. A.; Lippard, S. J. *J. Am. Chem. Soc.* **1982**, *104*, 133–136. (h) Brant, P.; Cotton, F. A.; Sekutowski, J. C.; Wood, T. E.; Walton, R. A. *J. Am. Chem. Soc.* **1979**, *101*, 6588–6593. (i) LaRue, W. A.; Liu, A. T.; San Fillipo, J. *Inorg. Chem.* **1980**, *19*, 315–320. (j) Lam, C. T.; Novotny, M.; Lewis, D. L.; Lippard, S. J. *Inorg. Chem.* **1978**, *17*, 2127–2133. (k) Rutherford, N. M.; Olmstead, M. M.; Balsch, A. L. *Inorg. Chem.* **1984**, *23*, 2833–2837. (l) Dewan, J. C.; Giandomenico, C. M.; Lippard, S. J. *Inorg. Chem.* **1981**, *20*, 4069–4074. (m) Cotton, F. A.; Dunne, T. G.; Wood, J. S. *Inorg. Chem.* **1965**, *4*, 318–325.

degree of bending of the isocyanide ligand "couples" to the C≡N stretching frequency and thereby gives rise to the breadth of the band. The aryl isocyanides do not show as low of a C≡N stretching frequency. Cotton has previously discussed in detail the valence bond vs. molecular orbital description of isocyanide binding in the complex $[Co(CNMe)_5]^+$.[11m]

Conclusions

The complexes described here contain isocyanide ligands in which metal–ligand π-back-bonding induces severe bending of the C–N–C linkage. These complexes are labile with respect to ligand substitution and ought to serve as sources of coordinatively unsaturated electron-rich metals with ligands that are reactive toward insertion reactions.

Experimental Section

All solvents were distilled from dark purple solutions of sodium benzophenone ketyl under a nitrogen atmosphere. All compounds were handled in a Vacuum Atmospheres Dri-Lab. All experiments were performed in sealed NMR tubes or ampules prepared and degassed on a high-vacuum line. *t*-BuNC and *i*-PrNC were purchased from Aldrich Chemical Co. PMe_3 was purchased from Strem Chemical Co. CN-2,6-xyl was purchased from Tridom/Fluka Chemical Co. The method of Ugi was used to prepare PhNC and $CNCH_2CMe_3$.[12a] EtNC was prepared as previously described from AgCN and EtI.[12b]

NMR spectra were obtained on a Bruker WH-400 instrument. NMR chemical shifts are reported in units of δ vs. residual C_6D_6 (7.150 for ^1H, 128.0 for ^{13}C) or external H_3PO_4 (for ^{31}P). Mass spectra were recorded on a Du Pont 490B mass spectrometer. IR spectra were recorded on a Perkin-Elmer 467 infrared spectrometer. Single-crystal diffraction studies were carried out on an Enraf-Nonius CAD-4 diffractometer or on a Picker FACS-1 diffractometer.

Preparation of $Fe(PMe_3)_2(CN\text{-}t\text{-}Bu)_3$. Into a 50-mL two-neck flask fitted with a rubber septum were weighed 0.30 g (2.36 mmol) of $FeCl_2$ and 0.172 g (7.09 mmol) of Mg. The flask was attached to a vacuum line, and PMe_3 (200 mm, 1.10 L, 300 K; 11.8 mmol) and THF (20 mL) were condensed in at 77 K. The flask was allowed to warm to room temperature for several minutes, and then the mixture was stirred in an ice bath (0 °C) for 1.5 h. Several color changes were noted during this period, ultimately producing a yellow-brown solution. This solution was transferred under nitrogen with a stainless-steel needle into a clean flask and *t*-BuNC (0.79 mL) condensed in at 77 K. The solution was stirred at 25 °C for 1 h, over which time a yellow-orange solution formed. The volatiles were removed under vacuum (10^{-4} mm, 25 °C), and the residue was extracted with 30 mL of hexane in the drybox. Removal of solvent under reduced pressure gave 0.425 g (40%) of bright yellow $Fe(PMe_3)_2(CN\text{-}t\text{-}Bu)_3$. Mass spectrum (20 eV): 457 (M^+), 381 ($M^+ - PMe_3$), 374 (M^+ – CNR), 305 ($M^+ - 2PMe_3$), 298 ($M^+ - PMe_3$ – CNR), 291 (M^+ – 2CNR), 222 ($M^+ - 2PMe_3$ – CNR), 215 ($M^+ - PMe_3$ – 2CNR), 208 (M^+ – 3CNR), 139 ($M^+ - 2PMe_3$ – 2CNR), 132 ($M^+ - PMe_3$ – 3CNR), 56 ($M^+ - 2PMe_3$ – 3CNR). IR (hexane, cm^{-1}): 1980 (vbr), 1800 (vbr). The time delay required for analysis precluded obtaining accurate analytical data for the complex. $^{31}P\{^1H\}$ NMR (C_6D_6): δ 42.08 (s). $^{13}C\{^1H\}$ NMR (C_6D_6): δ 20.69 (t, J = 12 Hz), 31.49 (s), 54.18 (s), 208.10 (t, J = 33 Hz).

Preparation of $Fe(PMe_3)_2(CNCH_2CMe_3)_3$. The preparation was identical with that above except that $CNCH_2CMe_3$ (3.5 equiv) was employed in place of *t*-BuNC, yielding 52% of crude product. Low-temperature recrystallization from hexane gave pure yellow crystalline product. Mass spectrum (20 eV): 499 (M^+), 423 ($M^+ - PMe_3$), 402 (M^+ – CNR), 347 ($M^+ - 2PMe_3$), 326 ($M^+ - PMe_3$ – CNR), 305 (M^+ – 2CNR), 250 ($M^+ - 2PMe_3$ – CNR), 229 ($M^+ - PMe_3$ – 2CNR), 208 (M^+ – 3CNR), 153 ($M^+ - 2PMe_3$ – 2CNR), 132 ($M^+ - PMe_3$ – 3CNR), 56 ($M^+ - 2PMe_3$ – 3CNR). $^{31}P\{^1H\}$ NMR (C_6D_6): δ 46.42 (s). $^{13}C\{^1H\}$ NMR (C_6D_6): δ 41.71 (t, J = 11 Hz), 45.57 (s), 49.51 (s), 71.46 (s), 196.26 (t, J = 27 Hz).

Preparation of $Fe(PMe_3)_2(CNPh)_3$. The preparation was identical with that above except that PhNC (3.25 equiv) was employed in place of *t*-BuNC and that the product crystallized directly from THF solution upon concentration. Yield: 0.537 g (44%). Mass spectrum (20 eV): 517 (M^+), 441 ($M^+ - PMe_3$), 414 (M^+ – CNR), 365 ($M^+ - 2PMe_3$), 338 ($M^+ - PMe_3$ – CNR), 311 (M^+ – 2CNR), 262 ($M^+ - 2PMe_3$ – CNR), 235 ($M^+ - PMe_3$ – 2CNR), 208 (M^+ – 3CNR), 159 ($M^+ - 2PMe_3$ – 2CNR), 132 ($M^+ - PMe_3$ – 3CNR), 56 ($M^+ - 2PMe_3$ – 3CNR). IR (THF, cm^{-1}): 1960 (vbr), 1720 (vbr). Anal. Calcd (found) for $FeP_2N_3C_{27}H_{33}$: C, 62.68 (63.01); H, 6.43 (6.48); N, 8.12 (8.29).

Preparation of $Fe(PMe_3)_2(CN\text{-}2,6\text{-}xyl)_3$ and $Fe(PMe_3)(CN\text{-}2,6\text{-}xyl)_4$. The preparation was identical with that above except that CN-2,6-xyl (3.25 equiv) was employed in place of CN-*t*-Bu. Evaporation of the THF solution gave bright red product (0.52 g) that was shown by ^1H NMR spectroscopy to be a 1:2 mixture of $Fe(PMe_3)_2(CN\text{-}2,6\text{-}xyl)_3$ and $Fe(PMe_3)(CN\text{-}2,6\text{-}xyl)_4$, which were separated by fractional crystallization from hexane as follows. The red solid was dissolved in THF and layered with hexane (1:3 v/v). A small amount of a gelatinous precipitate formed overnight and was separated by filtration. The mother liquor was evaporated (25 °C, 10^{-4} mm) and the residue taken up in hexane. Upon cooling to −78 °C, $Fe(PMe_3)(CN\text{-}2,6\text{-}xyl)_4$ crystallized from solution (yield 0.20 g, 14%). Reduction of the solvent volume yielded crystals of the product $Fe(PMe_3)_2(CN\text{-}2,6\text{-}xyl)_3$ (0.055 g, 4%). The low isolated yields reflect difficulties in the fractional crystallization rather than poor preparative yields. Data for $Fe(PMe_3)(CN\text{-}2,6\text{-}xyl)_4$ are as follows. IR (KBr, cm^{-1}): 1986, 1939 (br), 1868, 1828. Mass spectrum (20 eV): 656 (M^+), 580 ($M^+ - PMe_3$), 525 (M^+ – CNR), 449 ($M^+ - PMe_3$ – CNR). Anal. Calcd (found) for $FePN_4C_{39}H_{45}$: H, 6.91 (6.84); C, 71.34 (71.61); N, 8.53 (8.10). Data for $Fe(PMe_3)_2(CN\text{-}2,6\text{-}xyl)_3$ are as follows. IR (KBr, cm^{-1}): 2096 (br), 2057 (br), 1997 (sh). $^{13}C\{^1H\}$ NMR (C_6D_6): δ 20.15 (s), 21.57 (t, J = 13 Hz), 123.88 (s), 128.57 (s), 133.94 (s), 135.25 (s), 203.28 (t, J = 34 Hz). Mass spectrum (70 eV): 601 (M^+), 525 ($M^+ - PMe_3$), 470 (M^+ – CNR), 449 ($M^+ - 2PMe_3$), 394 ($M^+ - PMe_3$ – CNR), 339 (M^+ – 2CNR), 318 ($M^+ - 2PMe_3$ – CNR), 263 ($M^+ - PMe_3$ – 2CNR), 187 ($M^+ - 2PMe_3$ – 2CNR).

Preparation of $Fe(PMe_3)_2(CNMe)_3$. The preparation was identical with that above except that CNMe (3.5 equiv) was employed in place of CN-*t*-Bu. Concentration of the THF solution to ~5 mL followed by addition of hexane (~30 mL) produced a flocculent yellow-white precipitate that was removed by filtration. Removal of solvent from the mother liquor (25 °C, 10^{-4} mm) yielded 0.38 g (49%) of product that was recrystallized from THF/hexane. IR (THF, cm^{-1}): 2050 (br), 1920 (br), 1780 (br). The yellow crystals turned brown after storage under nitrogen for several days.

Attempted Preparation of $Fe(PMe_3)_2(CN\text{-}i\text{-}Pr)_3$. The preparation was identical with that above except that *i*-PrNC (3.3 equiv) was employed in place of CN-*t*-Bu. An IR spectrum of the orange THF solution showed bands at 2143 (m, free RNC), 2108 (m), and 1790 (br) cm^{-1}. Removal of the solvent under vacuum (10^{-4} mm) at 0 °C afforded an orange solid. Upon warming to 25 °C, the solid rapidly decomposed (~10 min) with the evolution of gas. The volatiles were trapped at 77 K, and 2 mL of C_6H_6 was condensed in. Analysis of a 1-μL sample on a $^1/_8$ in. × 10 ft 10% UC-W98/Chrom WAW column (60 °C) showed the presence of propene and PMe_3, but no *i*-PrNC.

Attempted Preparation of $Fe(PMe_3)_2(CNEt)_3$. The preparation was identical with that above except that EtNC (3.35 equiv) was employed in place of *t*-BuNC. Evaporation of the THF solvent left an intractable tarry black residue.

Photolysis of $Fe(PMe_3)_2(CNCH_2CMe_3)_3$ in the Presence of PMe_3. A 12-mg (0.024-mmol) sample of the iron complex was weighed into an NMR tube attached to a ground-glass joint and PMe_3 (13.3 mm, 67.5 mL, 300 K; 0.0481 mmol) plus 0.82 mL of C_6D_6 condensed in. The tube was sealed under vacuum. An ^1H NMR spectrum after 60 h in the dark showed no reaction. Irradiation with a 500-W medium-pressure Hg lamp through a 313-nm band-pass filter for 57 h showed the formation of a new product with ^1H NMR resonances for $Fe(PMe_3)_3(CNCH_2CMe_3)_2$ cited in Table I. The $^1P\{^1H\}$ NMR spectrum showed a new resonance at δ 29.28 (s).

Equilibrium Constant Measurements. The equilibria between the complexes $Fe(PMe_3)_2(CNR)_3$, $Fe(PMe_3)(CNR)_4$, and $Fe(CNR)_5$ were measured by treating a C_6D_6 solution (0.68 mL) of the tris(isocyanide) complex (30 mg, 0.0656 mmol) with 50 μL (0.589 mmol) of *t*-BuNC. After 10 h of standing, a ^1H NMR spectrum was recorded, and the integrated areas of the PMe_3 and *t*-BuNC resonances were used to calculate the equilibrium constants for eq 2 and 3.

In a similar experiment, $Fe(PMe_3)_2(CNCH_2CMe_3)_3$ (9 mg, 0.0180 mmol) and 10 μL (0.072 mmol) of $CNCH_2CMe_3$ were dissolved in 0.50 mL of C_6D_6 in a sealed NMR tube, and the integrated areas of the PMe_3 and $CNCH_2CMe_3$ resonances were used to determine K_1 and K_2 for this series of molecules after equilibrating for 35 h at 25 °C.

General Procedure for Structural Determinations. Following mounting of the crystal with epoxy on a glass fiber under nitrogen, the sample was coated with epoxy. Alternatively, the crystal was wedged into a quartz capillary. Lattice constants were obtained from 25 centered reflections with values of χ between 0 and 60° (15 reflections with the FACS1 diffractometer). Cell reduction with the program TRACER revealed the crystal system. Data were collected on the crystal in accord with the

(12) (a) *Organic Syntheses*; Baumgarten, H. E., Ed.; Wiley: New York, 1973; Collect. Vol. V, p 1060. (b) *Organic Syntheses*; Rabjohn, N., Ed.; Wiley: New York, 1963; Collect. Vol. IV, pp 438–440.

Table VII. Positional Parameters for $Fe(PMe_3)(CN\text{-}2,6\text{-}xyl)_4$

atom	x	y	z
Fe	0.28240 (4)	0.23270 (8)	0.43748 (4)
P1	0.32726 (8)	0.0561 (2)	0.50660 (8)
N1	0.2230 (2)	0.4858 (5)	0.3551 (3)
N2	0.3930 (2)	0.4003 (5)	0.5455 (3)
N3	0.3058 (2)	0.1066 (5)	0.3106 (2)
N4	0.1557 (2)	0.1498 (5)	0.4546 (2)
C1	0.2453 (3)	0.3851 (6)	0.3858 (3)
C2	0.3503 (2)	0.3351 (6)	0.5033 (3)
C3	0.2963 (3)	0.1577 (6)	0.3599 (3)
C4	0.2053 (3)	0.1867 (6)	0.4460 (3)
C5	0.1971 (3)	0.6118 (6)	0.3250 (3)
C6	0.2175 (3)	0.6660 (7)	0.2716 (3)
C7	0.1899 (3)	0.7909 (7)	0.2422 (3)
C8	0.1469 (3)	0.8570 (7)	0.2659 (4)
C9	0.1281 (3)	0.8000 (7)	0.3182 (3)
C10	0.1527 (3)	0.6768 (6)	0.3497 (3)
C11	0.2662 (3)	0.5911 (8)	0.2478 (4)
C12	0.1331 (3)	0.6145 (8)	0.4081 (4)
C13	0.4452 (2)	0.4869 (6)	0.5823 (3)
C14	0.4846 (3)	0.4643 (7)	0.6567 (3)
C15	0.5378 (3)	0.5502 (8)	0.6915 (3)
C16	0.5518 (3)	0.6539 (8)	0.6545 (4)
C17	0.5116 (3)	0.6798 (7)	0.5817 (4)
C18	0.4568 (3)	0.5969 (6)	0.5423 (3)
C19	0.4688 (3)	0.3527 (8)	0.6972 (3)
C20	0.4120 (3)	0.6194 (7)	0.4637 (3)
C21	0.3015 (3)	0.0545 (6)	0.2435 (3)
C22	0.2545 (3)	0.1086 (6)	0.1769 (3)
C23	0.2527 (3)	0.0529 (7)	0.1120 (3)
C24	0.2934 (3)	−0.0510 (8)	0.1110 (3)
C25	0.3388 (3)	−0.1018 (7)	0.1769 (3)
C26	0.3445 (3)	−0.0503 (7)	0.2444 (3)
C27	0.2085 (4)	0.2186 (8)	0.1785 (4)
C28	0.3947 (4)	−0.1034 (9)	0.3167 (4)
C29	0.0938 (3)	0.0817 (6)	0.4219 (3)
C30	0.0491 (3)	0.1182 (7)	0.3506 (3)
C31	−0.0118 (3)	0.0494 (8)	0.3215 (3)
C32	−0.0267 (3)	−0.0510 (8)	0.3605 (4)
C33	0.0185 (3)	−0.0840 (8)	0.4306 (4)
C34	0.0799 (3)	−0.0196 (6)	0.4623 (3)
C35	0.0667 (3)	0.2257 (8)	0.3087 (4)
C36	0.1302 (3)	−0.0551 (8)	0.5380 (3)
C37	0.3258 (3)	0.0580 (7)	0.5984 (3)
C38	0.4154 (3)	0.0248 (4)	0.5272 (4)
C39	0.2892 (3)	−0.1035 (7)	0.4710 (3)
C40	1.0477 (3)	0.4125 (8)	0.4983 (4)
C41	0.9850 (4)	0.4035 (8)	0.4466 (4)
C42	1.0633 (3)	0.5087 (8)	0.5526 (4)

parameters in Table II. Patterson map determination of the iron position allowed solution of the structure, and subsequent difference Fourier and full-matrix least-squares refinement converged to the final solution. The Molecular Structure Corp. SDP package was used for solution and refinement of the structure.[13]

X-ray Structural Determination of $Fe(PMe_3)_2(CNCH_2CMe_3)_3$. Well-formed orange crystals of the complex were grown by slow evaporation of a saturated hexane solution in a sealed tube at −20 °C and mounted in a sealed capillary. Possible monoclinic space groups based upon systematic absences included $C2$, Cm, and $C2/m$. $C2$ was chosen since $Z = 4$ represents a general position and the Patterson map showed an arbitrary value for the y coordinate of the iron atom. The correctness of this acentric choice was confirmed by successful solution of the structure. No attempt was made to place the methyl or methylene hydrogens. A final difference Fourier map and peak search failed to show any peaks in the position to represent a rotational disorder of the CMe_3 groups. Final anisotropic refinement of all atoms was carried out and converged to the values of R_1 and R_2 listed in Table II. Changing the chirality of the crystal gave a slightly worse R_1 index (0.069). Table III contains the relevant bond distances and angles, and Table IV includes the positional parameters.

(13) $R_1 = [\sum||F_o| - |F_c||]/[\sum|F_o|]$; $R_2 = [\sum w(|F_o| - |F_c|)^2]^{1/2}/[\sum wF_o^2]$, where $w = [\sigma^2(F_o) + (pF_o^2)^2]^{1/2}$ for the non-Poisson contribution weighting scheme. The quantity minimized was $\sum w(|F_o| - |F_c|)^2$. Source of scattering factors f_o, f', f'': Cromer, D. T.; Waber, J. T. *International Tables for X-Ray Crystallography*; Kynoch: Birmingham, England, 1974; Vol. IV, Tables 2.2B, 2.3.1.

Table VIII. C–N–C Bond Angles in Various Isocyanide Complexes

molecule	C–N–C, deg	ref
$Fe(PMe_3)_2(CNCH_2CMe_3)_3$	140, 146, 166	this work
$Fe(PMe_3)_2(CNPh)_3$	131.8, 180.0	this work
$Fe(PMe_3)_2(CN\text{-}2,6\text{-}xyl)_3$	147.7, 149.8, 161.3	this work
$Fe(PMe_3)(CN\text{-}2,6\text{-}xyl)_4$	145.1, 166.7, 167.9, 174.5[a]	this work
$Fe(CN\text{-}t\text{-}Bu)_5$[b]	133.1, 134.6, 169.2, 151.6,[a] 177.1[a]	5, 7
	135.2, 136.9, 166.3, 158.1,[a] 165.0[a]	
$Ru(PPh_3)(CN\text{-}t\text{-}Bu)_4$	129, 131, 167,[a] 172[a]	6, 7
$Mo(CNMe)_2(dppe)_2$	156	11a
$Co_2(CN\text{-}t\text{-}Bu)_8$	130.8,[c] 154	6
$Pd_3(CN\text{-}c\text{-}Hx)_6$	128.9,[c] 170.2	11b
$Pt_3(CN\text{-}t\text{-}Bu)_6$	170,[d] 140[c]	11c
$Ni_4(CN\text{-}t\text{-}Bu)_7$	163,[c] 171	11d
$Pt_7(CN\text{-}2,6\text{-}xyl)_{12}$	169[d]	11e
$(C_5Me_5)_2V(CN\text{-}c\text{-}Hx)$	175	11f
$[Cr(CN\text{-}t\text{-}Bu)_7]^{2+}$	176.4–179.1[d]	11g
$[Mo(CNMe)_7]^{2+}$	176.0–178.7[d]	11h
$[W(CN\text{-}t\text{-}Bu)_7]^{2+}$	172.0–178.0[d]	11i
$[Mo(CN\text{-}t\text{-}Bu)_6Br]^{+}$	168.2, 173.0, 177.0, 179.7	11j
$[Pd_2(CNMe)_4I_2]^{2+}$	177.0, 177.2, 177.5, 178.0	11k
$[Mo(CN\text{-}t\text{-}Bu)_4(t\text{-}BuHNCCNH\text{-}t\text{-}Bu)(CN)]^{+}$	172.6, 173.2	11l
$[Co(CNMe)_5]^{+}$	177, 173	11m

[a] Axial ligand in trigonal bipyramid. [b] Two independent molecules per unit cell. [c] Bridging isocyanide. [d] Average value for terminal isocyanides.

X-ray Structural Determination of $Fe(PMe_3)_2(CNPh)_3$. Well-formed orange crystals of the compound were prepared by slow evaporation of a THF/hexane solution and mounted in epoxy. After manual alignment on the Picker FACS-1 diffractometer, data were collected in accord with the parameters in Table II. The centric monoclinic space group $C2/c$ was chosen on the basis of systematic absences. A Patterson map solution showed the iron lying on a 2-fold symmetry axis, and differecne Fourier maps revealed one isocyanide lying along the 2-fold axis and the remaining unique PMe_3 and PhNC ligands. A difference Fourier map was used to place the methyl hydrogens on the phosphine ligands, and phenyl hydrogens were placed at idealized locations. Full-matrix least-squares refinement was carried out with fixed positions and thermal parameters ($B = 5.0$ Å^2) for the hydrogen atoms. Table III contains the relevant bond distances and angles, and Table V includes the positional parameters.

X-ray Structural Determination of $Fe(PMe_3)_2(CN\text{-}2,6\text{-}xyl)_3$. Well-formed red crystals of the compound were prepared by slow evaporation of a hexane solution and mounted in epoxy. The data were corrected for a decay of 4.3%. The unique monoclinic space group $P2_1/c$ was chosen on the basis of systematic absences. A Patterson map was used to locate the iron and the two phosphorus atoms in general positions, and difference Fourier maps revealed the remaining atoms. A difference Fourier map was used to place the methyl hydrogens, and aromatic hydrogens were placed at idealized locations. Full-matrix least-squares refinement was carried out with fixed positions and thermal parameters ($B = 5.0$ Å^2) for the hydrogen atoms. Table III contains the relevant bond distances and angles, and Table VI includes the positional parameters.

X-ray Structural Determination of $Fe(PMe_3)(CN\text{-}2,6\text{-}xyl)_4$. Well-formed red crystals of the compound were prepared by evaporation of a benzene/hexane solution and mounted in epoxy. The data were corrected for 15.9% decay. The unique monoclinic space group $P2_1/c$ was chosen on the basis of systematic absences. A Patterson map solution showed the iron in a general position, and difference Fourier maps revealed the remaining atoms. A difference Fourier map showed a benzene of recrystallization lying on a center of symmetry. Following anisotropic refinement, a difference Fourier map was used to place the methyl hydrogens, and phenyl hydrogens were placed at idealized locations. Full-matrix least squares refinement was carried out with fixed positions and thermal parameters ($B = 5.0$ Å^2) for the hydrogen atoms. Table III contains the relevant bond distances and angles, and Table VII includes the positional parameters.

Acknowledgment is made to the U.S. Department of Energy (Grant FG02-86ER13569) and to the Petroleum Research Fund, administered by the American Chemical Society, for their partial support of this work. W.D.J. also thanks the Alfred P. Sloan and Camille and Henry Dreyfus Foundations for awards.

Registry No. I, 108121-43-3; II, 108121-44-4; III, 108121-45-5; IV,

108121-48-8; $Fe(PMe_3)_2(CNMe)_3$, 108121-41-1; $Fe(PMe_3)_2(CN\text{-}t\text{-}Bu)_3$, 108121-42-2; $Fe(PMe_3)(CN\text{-}t\text{-}Bu)_4$, 108121-46-6; $Fe(PMe_3)(CNCH_2CMe_3)_4$, 108121-47-7; $Fe(PMe_3)_3(CNCH_2CMe_3)_2$, 108121-49-9; $Fe(CN\text{-}t\text{-}Bu)_5$, 66415-98-3; $Fe(CNCH_2CMe_3)_5$, 108121-50-2; $FeCl_2$, 7758-94-3; t-BuNC, 7188-38-7; $CNCH_2CMe_3$, 72443-18-6.

Supplementary Material Available: For the four structure determinations, listings of bond distances and angles, fractional coordinates of placed hydrogen atoms, and anisotropic thermal parameters (27 pages); listings of calculated and observed structure factors (85 pages). Ordering information is given on any current masthead page.

Contribution from the Applied Sciences and Microgravity Section, Jet Propulsion Laboratory, California Institute of Technology, Pasadena, California 91109, and Inorganic and Structural Chemistry Group (INC-4) and Computing and Communication Division (C-8), Los Alamos National Laboratory, University of California, Los Alamos, New Mexico 87545

Assignment of the Rhodium–Rhodium Stretching Frequency in $Rh_2(O_2CCH_3)_4L_2$ Complexes and the Crystal and Molecular Structure of $[C(NH_2)_3]_2[Rh(O_2CCH_3)_4Cl_2]$. Relationship between Vibrational Spectra and Structure

Vincent M. Miskowski,*† Richard F. Dallinger,‡ Gary G. Christoph,§ David E. Morris,§ George H. Spies,∥ and William H. Woodruff*§

Received February 12, 1986

The resonance Raman spectra of salts of $[Rh_2(OAc)_4X_2]^{2-}$ (X = Cl^-, Br^-, I^-; OAc = O_2CCH_3) obtained by using ultraviolet laser excitation, and the structure of the salt $[C(NH_2)_3]_2[Rh_2(OAc)_4Cl_2]$, are reported. The salt crystallizes with two molecules per tetragonal (space group No. 87, $I4/m$) unit cell; a = 8.564 (1) Å and c = 13.955 (1) Å (T = −47 (1) °C). Least-squares refinement of 1395 unique reflections led to a final weighted $R(F^2)$ value of 0.053 ($R(F)$ = 0.030). Significant results of the structure determination are the Rh–Rh, Rh–Cl, and Rh–O distances of 2.3959 (3), 2.5853 (6), and 2.042 (1) Å, respectively. Ultraviolet resonance Raman results reveal that the rhodium–rhodium stretching motion of $[Rh_2(OAc)_4I_2]^{2-}$ is the predominant contributor to a normal vibrational mode observed at 314 cm^{-1}, rather than at 170 cm^{-1} as suggested in a previous assignment. In the bromide complex the analogous mode appears at 286 cm^{-1}. Simplified vibrational calculations yield a force constant of 2.60 mdyn/Å for the Rh–Rh bond in the iodide complex. This force constant is consistent with a new comprehensive relationship between force constants and bond distances, while a force constant based upon ν(Rh–Rh) ≈ 170 cm^{-1} is not.

Rhodium(II) acetate, $Rh_2(OAc)_4$, with its axial adducts and substituted carboxylate variants, is the prototypical example of a strong metal–metal single bond.[1] Yet, one of the most fundamental indicators of bond strength, the metal–metal stretching frequency (and the derived force constant of the Rh–Rh bond), has proved difficult to establish. Early Raman investigations of $Rh_2(OAc_2)_4L_2$ complexes, using laser excitation in the visible region of the spectrum, led to assignment of ν(Rh–Rh) to either of two polarized lines near 340 and 170 cm^{-1}.[2,3] The rationale for this assignment was largely that these were the strongest lines in the low-frequency Raman spectra. The 340-cm^{-1} assignment was recently eliminated by one of us,[4] who, with others, established that the 340-cm^{-1} vibration was clearly due to the totally symmetric ν[Rh–O(carboxylate)] stretching mode. The 170-cm^{-1} line could not be as thoroughly characterized at that time, and it was settled on as the "preferred" assignment, given the available possibilities. This assignment was nonetheless somewhat disturbing, as it implied[4] a large deviation from well-established empirical correlations (such as Badger's rule[5] and more recent relationships[6]) relating bond lengths and force constants for single metal–metal bonded compounds. Some reasons this might occur were suggested.[4] However, subsequent correlations[6] (vide infra) extending the empirical data to include all types and orders of bonding predict a symmetric Rh–O stretching frequency of 347 cm^{-1}, in good agreement with the Rh–O assignment noted above, but a Rh–Rh stretching frequency of 282 cm^{-1}. Clearly, the inconsistency of the ~170-cm^{-1} ν(Rh–Rh) assignment is too serious to be ignored. Either there is a complete breakdown in the general relationship between metal–metal bond length and stretching force constant for $Rh_2(OAc)_4$ or the assignment is wrong.

Our strategy in reexamining the Raman spectroscopy of $Rh_2(OAc)_4L_2$ was to choose complexes and laser excitation frequencies that offered the chance of lending strong resonance enhancement to vibrational modes containing large contributions from the Rh–Rh stretching coordinate. The $\sigma \rightarrow \sigma^*$ transitions directly involving the Rh–Rh bond are probably at too high energy to be near the frequency of available CW laser lines in the near-ultraviolet region (vide infra). Accordingly, we chose to tune the energy of the σ(Rh–L) → σ^*(Rh–Rh) transition, which should enhance both the Rh–L and Rh–Rh stretches, to be near our ultraviolet laser lines by judicious choice of the axial ligand L. Axial ligands examined included Cl^-, Br^-, I^-, and CH_3CN. The iodide complex proved to have its σ(Rh–L) → σ^*(Rh–Rh) transition close enough to laser lines near 350 nm to accomplish our objectives.

Reliable structural interpretation of the vibrational data requires knowledge of the structure of the specific salts involved. Because the solid-state spectra of the halide complexes examined in this study were taken on the guanidinium salts of $[Rh_2(OAc)_4X_2]^{2-}$, the crystal structure of the guanidinium salt of $[Rh_2(OAc)_4Cl_2]^{2-}$ was determined for comparison to existing structural data for $[Li(OH_2)_4X_2]$ salts in order to establish that the structural parameters of the $[Rh_2(OAc)_4X_2]^{2-}$ complex are not strongly dependent on counterion. The structural determination also serves to check the extraordinarily long Rh–Rh distance of 2.49 Å reported by Nefedor et al., as opposed to 2.397 Å found in the work cited above.[4] Such a variation is most unexpected from earlier work on these compounds and, if correct, would suggest that the Rh–Rh bond potential is very flat and the minimum easily influenced by the environment and nature of the counterions. This

* To whom correspondence should be addressed.
† California Institute of Technology.
‡ Department of Chemistry, Wabash College, Crawfordsville, IN 47933.
§ University of California.
∥ Present address: Department of Chemistry, Iowa State University, Ames, IA 50010.

(1) Cotton, F. A.; Walton, R. A. *Multiple Bonds between Metal Atoms*; Wiley-Interscience: New York, 1982.
(2) Ketteringham, A. P.; Oldham, C. *J. Chem. Soc., Dalton Trans.* **1973**, 1067.
(3) (a) Kharitonov, Y. Y.; Mazo, G. Y.; Knyazeva, N. A. *Russ. J. Inorg. Chem. (Engl. Transl.)* **1970**, *15*, 739–740. (b) San Filippo, J., Jr.; Sniadoch, H. J. *Inorg. Chem.* **1973**, *12*, 2326–2333.
(4) Miskowski, V. M.; Schaefer, W. P.; Sadeghi, B.; Santarsiero, B. D.; Gray, H. B. *Inorg. Chem.* **1984**, *23*, 1154–1162.
(5) (a) Badger, R. M. *J. Chem. Phys.* **1934**, *2*, 128; **1935**, *3*, 710. (b) Hershback, D. R.; Laurie, V. W. *J. Chem. Phys.* **1961**, *35*, 458.
(6) Woodruff, W. H., to be submitted for publication in *J. Am. Chem. Soc.*

0020-1669/87/1326-2127$01.50/0